Supplemental material for

Coordination of transcriptional and translational regulations in human cells infected by *Listeria monocytogenes*

Vinko Besic, Fatemeh Habibolahi, Benoît F. Noël, Sebastian Rupp, Auguste Genovesio and Alice Lebreton

This document includes Supplemental Figures S1 to S10.

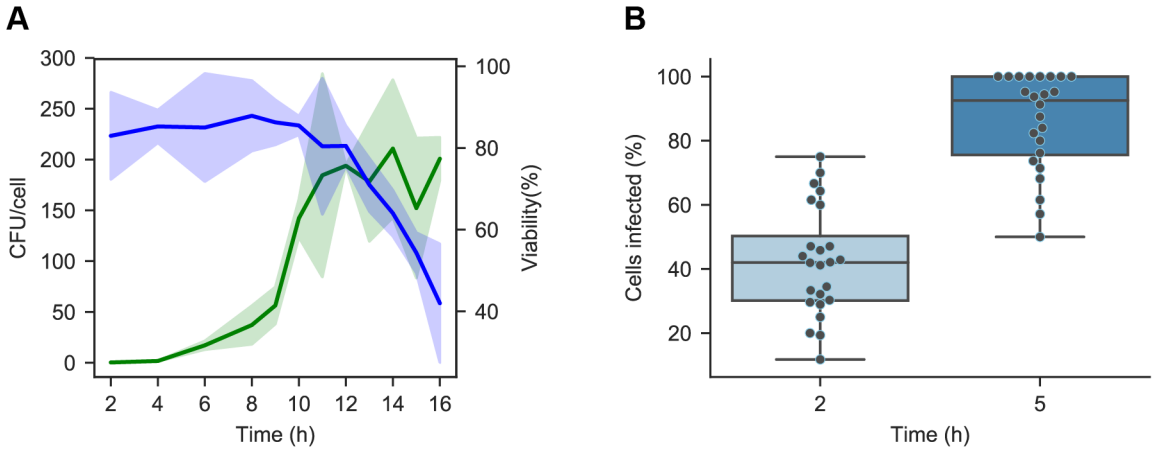

Figure S1. Assessment of infection kinetics and homogeneity. (**A**) The average number of bacteria per cell (CFU/cell, in green) and percentage of viable cells (Viability, in blue) were quantified over a 16-hour infection time course of LoVo cells, using an initial MOI of 30. CFUs were enumerated by plating serial dilutions on BHI-agar medium after cell lysis. Viability was assessed by live-dead staining using Trypan blue. Coloured bands in lighter shade indicate standard deviation. (**B**) Infection homogeneity was assessed by counting GFP-positive bacteria within each cell on microscopy slides, in 25 fields of vision per time-point. Cells were enumerated by counting DAPI-stained nuclei, and their contours were defined by revealing F-actin with Acti-Stain 670 fluorescent phalloidin. A cell was considered infected if it contained more than one bacterium.

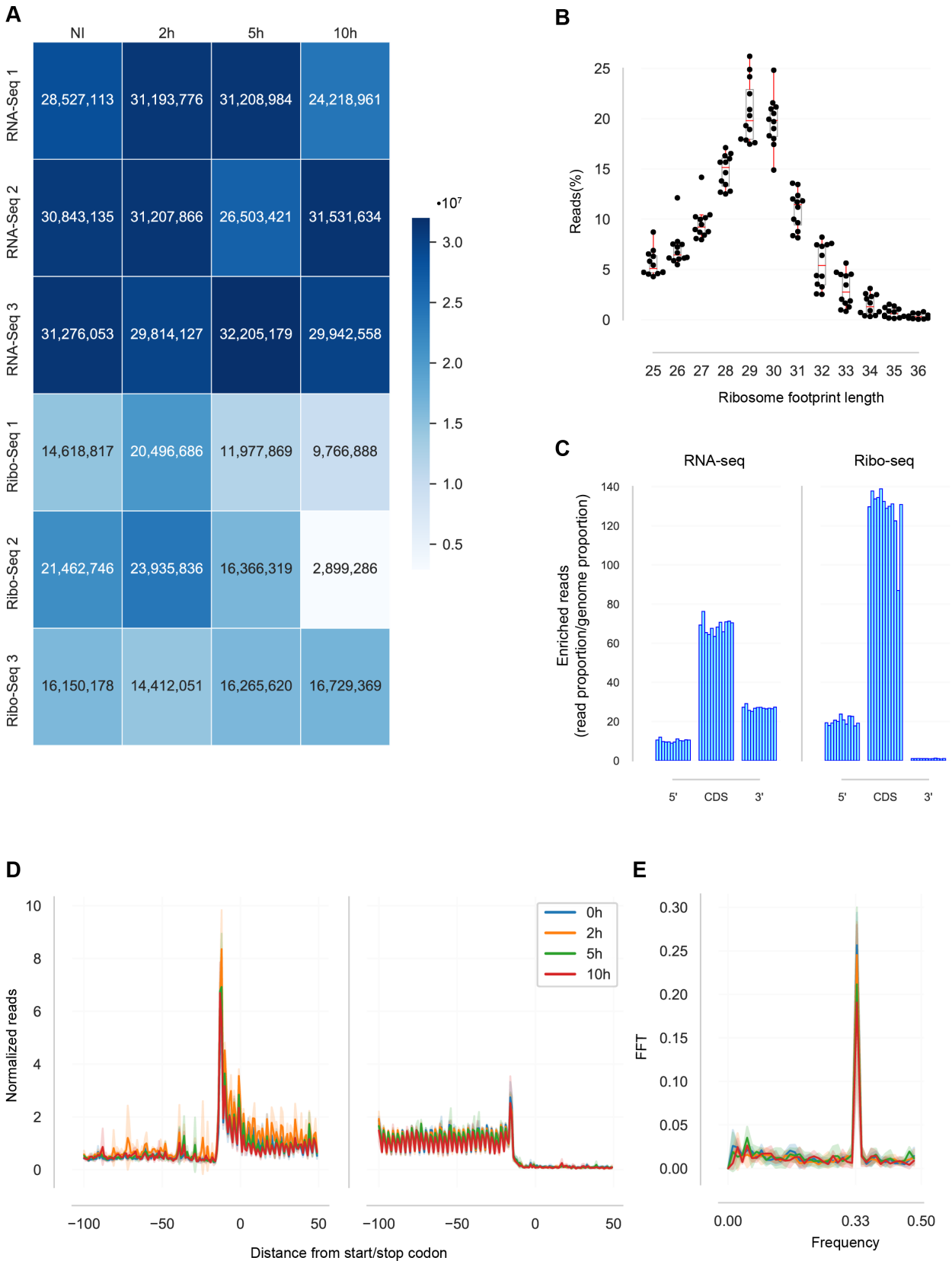

Figure S2. Quality controls of the RNA-seq and Ribo-seq data. (**A**) Number of uniquely mapped reads in each dataset reported in the present study. (**B**) Distribution of RFP read length. Each dot represents one of the Ribo-seq datasets. (**C**) Proportion of uniquely mapped reads matching to 5'-UTR, coding sequences (CDS) or 3'-UTRs in all transcripts across the RNA-seq (*left*) and Ribo-seq datasets (*right*) (**D**) Position of the 5'-end of sequenced RFPs relative to translation initiation sites (TIS) and stop codons in mRNAs. For

each position within a 150-nucleotide region around the TIS or the stop codon, the counts of 5'-ends of RFP reads matching this position were summed across all transcripts in each dataset and normalized by the number of transcripts. Read 5'-ends were previously reported to match around 12-13 upstream of the ribosome A site, thus the signals resulting from ribosomes scanning CDSs typically start 12 nucleotides upstream of the TIS and terminate 12 nucleotides upstream of the stop codon[1]. (**E**) Codon periodicity of RFP reads in coding sequences. The signal decomposition by fast Fourier transform (FFT) of the average counts on open reading frames highlights a sharp peak at 0.33 frequency, indicative of a three-nucleotide periodicity in the RFP reads, consistent with ribosomes scanning the coding sequence during translation elongation. The colour code is as in (**D**).

1. Ingolia NT, Ghaemmaghami S, Newman JRS, Weissman JS. Genome-wide analysis *in vivo* of translation with nucleotide resolution using ribosome profiling. Science 2009; 324:218–23.

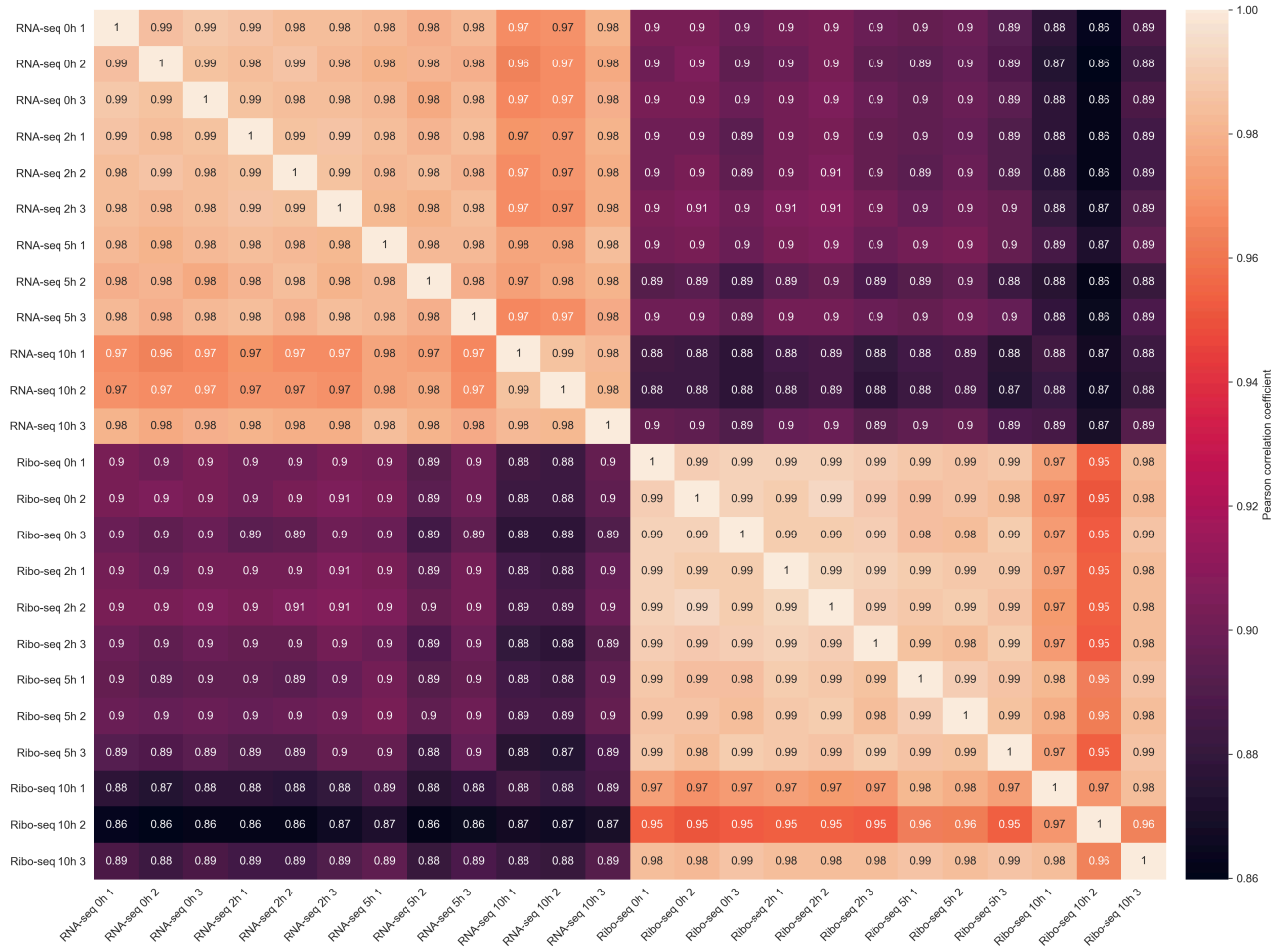

Figure S3. Correlative analysis of RNA-seq and Ribo-seq replicates. For each pair of RNA-seq or Ribo-seq samples, Pearson's correlation coefficient of the Reads Per Kilobase of transcript, per Million mapped reads (RPKM) value for each gene was calculated. Lighter shades indicate higher correlation. Note that the Ribo-seq 10 h sample #2 stood out as an outlier, confirming our choice to exclude it for subsequent analysis. Other samples showed high correlation across RNA-seq experiments on the one hand, Ribo-seq experiment on the other hand.

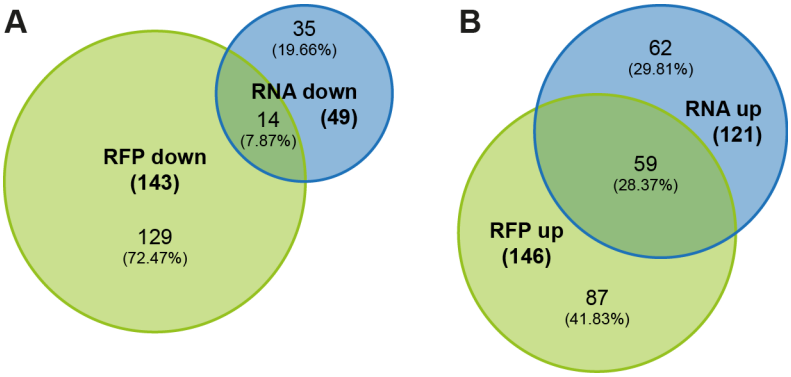

Figure S4. Overlap between differentially-regulated genes in the RNA-seq and Ribo-seq datasets between 2 and 5 h post-infection. The Venn diagrams highlight the number of differentially-regulated genes (DRGs with $p_{adj} < 0.05$ and FC > 1.5) in the RNA-seq (RNA, in blue) and Ribo-seq (RFP, in green) datasets, and their overlap. (**A**) down-regulated genes; (**B**) up-regulated genes. Percentages indicate the proportion out of the total number of genes on each panel. FC, fold change; p_{adj}, adjusted *p*-value [DESeq false discovery rate (FDR)].

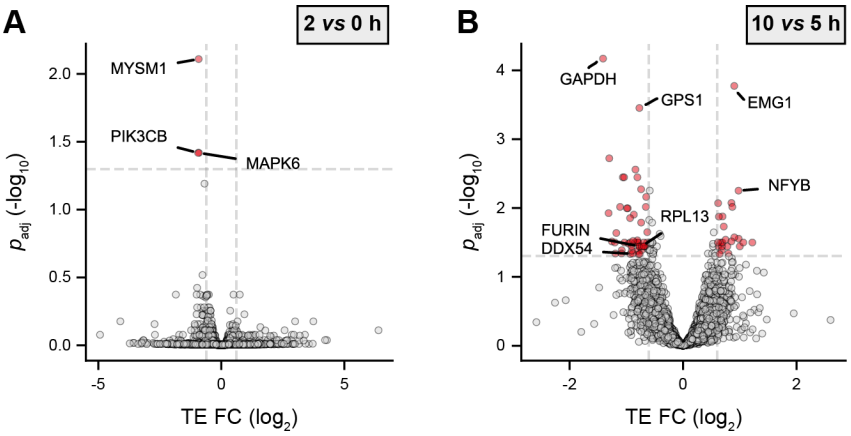

Figure S5. Variations in translation efficiencies during infection. The volcano plots highlight genes being significantly up- (*right*) or down- (*left*) regulated in translation efficiency (TE) at (**A**) 2 h p.i. compared to non-infected cells or (**B**) 10 h vs 5 h p.i. Data points coloured in red represent genes with an adjusted *p*-value below 0.05 (above dashed grey horizontal line; $-\log_{10} p_{adj} = 1.3$) and a FC below or above 1.5 (vertical dashed grey lines; $\log_2$ FC = ± 0.58). Data from three independent replicates (except for RFPs at 10 h). FC, fold change; p_{adj}, adjusted *p*-value.

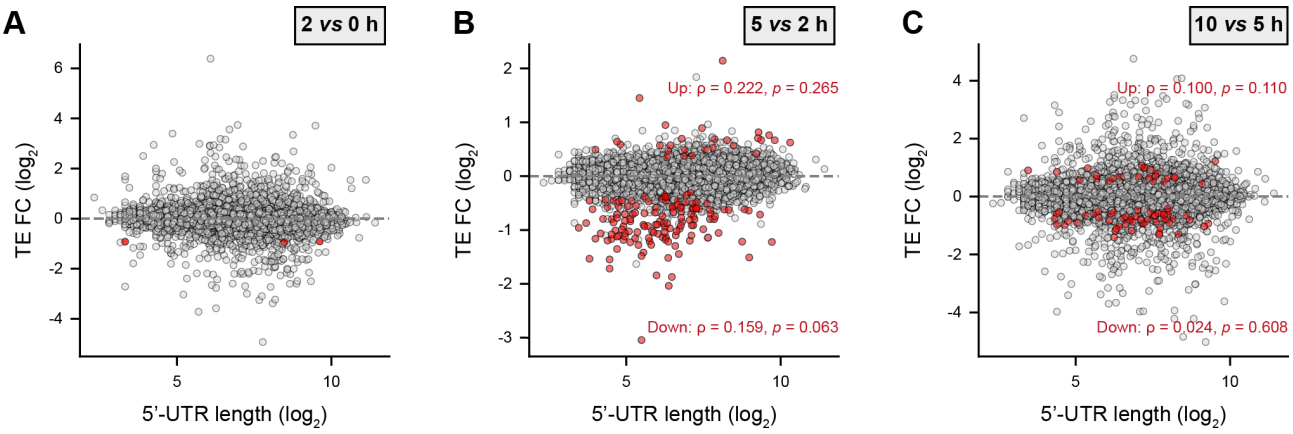

Figure S6. Correlation of changes in translational efficiency with 5'-UTR length. The $\log_2$ fold change (FC) of translational efficiencies (TE) between successive time-points of infection, calculated with Riborex, were plotted against the corresponding 5'-UTR length computed for each transcript with MANE Select annotation in Ensembl. Genes with an adjusted *p*-value on TE FC below 0.05 are highlighted in red. The Spearman's rank correlation coefficients (ρ) and *p*-value for these significantly up- or down-regulated genes is indicated.

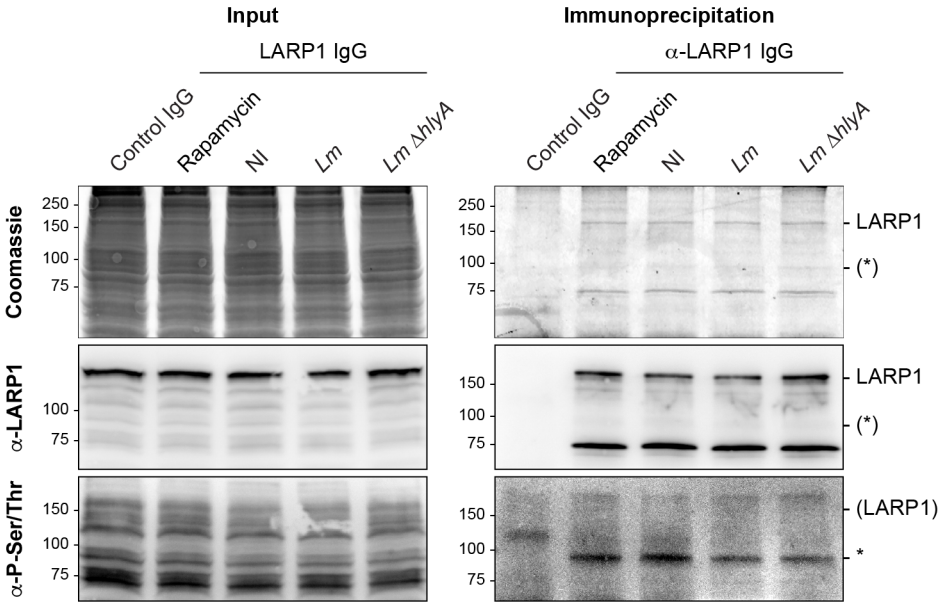

Figure S7. Phosphorylation status of LARP1 in LoVo cells. LARP1 was immunoprecipitated from LoVo cells that were infected or not for 5 h with *Lm* wild-type or with the *ΔhlyA* mutant strain, or treated for 3 h with 100 nM of rapamycin. Input and purified fractions were analysed by colloidal Coomassie staining (*top panel*) or by immunoblotting against LARP1 (*middle panel*) or using a total anti phospho-serine/threonine antibody (*bottom panel*).

Note that whereas LARP1 appeared unphosphorylated in all samples, we observed that an unknown phoshoprotein of ~90 kDa (*, *lower panel*) co-immunoprecipitated with LARP1 in non-infected cells and in lower amounts (46% of non-infected) upon infection with either the wild-type or the *ΔhlyA* strains. The abundance and/or phosphorylation status of this protein in the co-immunoprecipitation was scarcely affected by rapamycin treatment (91% of non-infected), suggesting that it might be mTOR-independent. Identifying the nature of this LARP1-associated phosphoprotein and assessing whether it plays any role in the translation of TOP-containing transcripts in LoVo cells could represent a path for future mechanistic investigation of the translational regulations we observed in response to *Lm* infection.

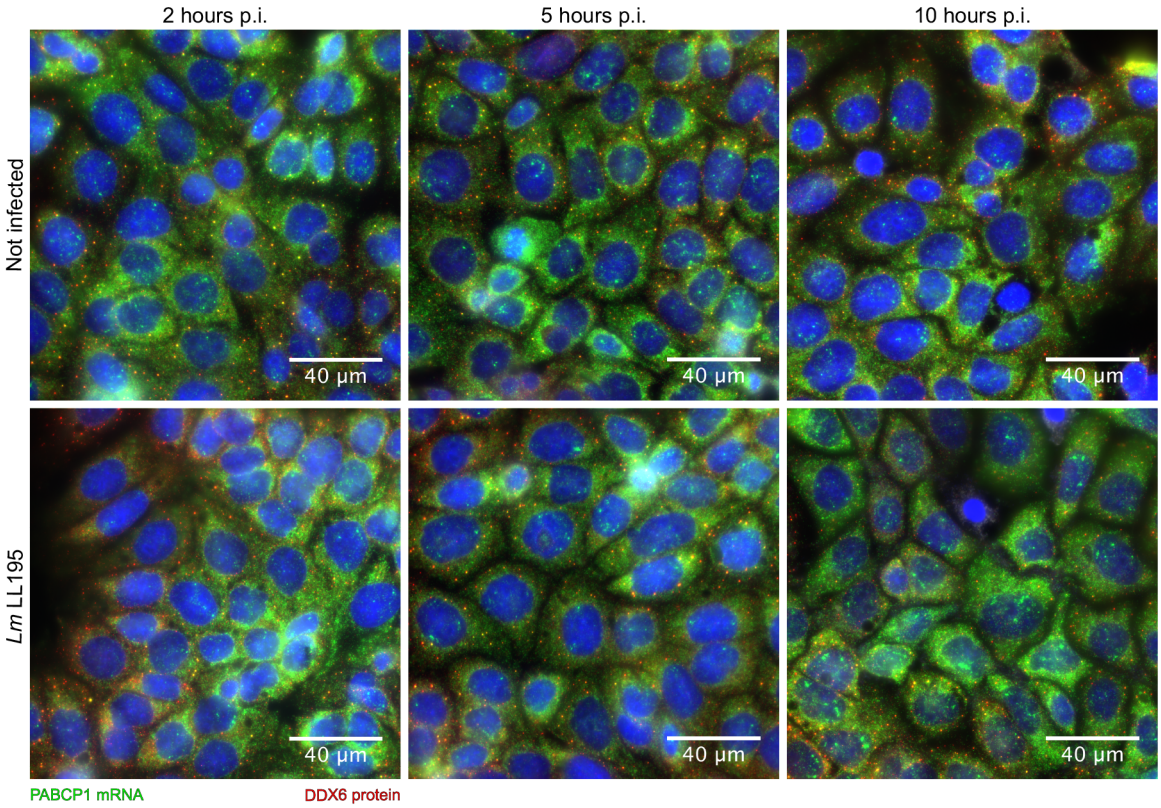

Figure S8. Localisation of *PABPC1* mRNA in LoVo cells infected or not with *Listeria monocytogenes*. LoVo cells were infected with *Lm* LL195 for 2, 5 or 10 h before fixation. The localisation of *PABPC1* mRNA was revealed by FISH (green), and that of P-bodies by immunofluorescence against DDX6 (red). Nuclei were stained with DAPI (blue).

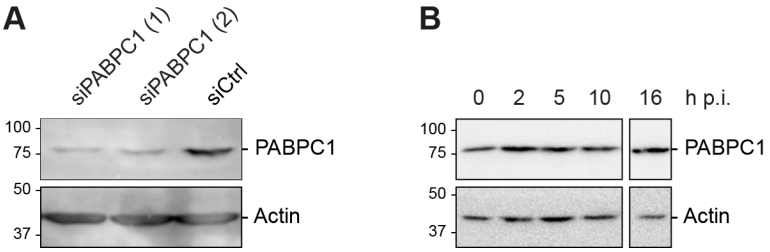

Figure S9. Assessment of PABPC1 protein levels upon transfection by siRNA or infection. PABPC1 and β-actin were revealed by immunoblotting. (**A**) *PABPC1* silencing by siRNAs. LoVo cells were transfected for 48 hours with siRNAs against *PABPC1* (siPABPC1 (1) and (2)) or with a scramble siRNA (siCtrl). (**B**) PABPC1 protein levels during infection. LoVo cells were infected for 0 to 10 h by *Lm* LL195 using a MOI of 30, or for 16 h using a MOI of 5.

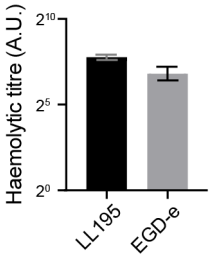

Figure S10. Haemolytic properties of *Listeria monocytogenes* strains LL195 and EGD-e. Data represent the means and standard deviations from three independent experiments.